Mixed Matrix Membranes Using SAPO-34/APMDES/PES for Carbon Dioxide/Methane Separation

Kiamehr, Yaser; Naser, Iraj*[+]; Rafizadeh, Mehdi
Department of Chemical Engineering, South Tehran Branch, Islamic Azad University, Tehran, I.R. IRAN

Mohammadi, Amir H.*[•]
Institut de Recherche en Génie Chimique et Pétrolier (IRGCP), Paris Cedex, FRANCE

ABSTRACT: *Among various CO_2-mitigation technologies, membrane-based technology has offered a more energy-efficient and eco-friendly process for CO_2 separation from large emission sources Despite the predominance of polymeric membranes in the CO_2/CH_4 separation, the tradeoff limitation between membrane selectivity and permeability hinders a good separation performance of these membranes Mixed matrix membranes can offer a dramatic improvement to overcome this shortcoming In this study, polyethersulfone (PES) mixed matrix membranes incorporated with small pore zeolite were proposed for CO_2/CH_4 separation SAPO-34 zeolite was used as inorganic fillers to enhance gas selectivity 3 3- aminopropylmethyldiethoxysilane (APMDES) was proposed to modify SAPO-34 zeolite before adding into asymmetric PES MMMs. The mixed matrix membranes were then characterized by FTIR, TGA, SEM, and gas permeation analysis. The separation results revealed that the increment of temperature from 30 °C to 50 °C reduced the CO_2/CH_4 separation factor while increasing feed pressure from 3 bar to 15 and the increment of CO_2 feed composition from 15 to 42.5 vol% increased the separation factor of PES/SAPO-34/APMDES. The DoE results showed that the feed pressure was the most significant process parameter that intensely affected the CH_4 permeance, CO_2 permeance, and CO_2/CH_4 separation factor. The synthesized MMMs in this study showed competitive CO_2/CH_4 separation performance compared with reported state-of-the-art PES-based membranes in pure gas permeation tests.*

KEYWORDS: *Mix matrix membrane; SAPO-34; Polyethersulfone; CO_2 separation.*

INTRODUCTION

Gas separation membrane technology has been receiving increasing attention because of its potential for reducing the environmental impact and the costs of industrial processes. The separation of CO_2 from CH_4

***** *To whom correspondence should be addressed.*
+ *E-mail*: *Iraj.nase.r@yahoo.com*
● *Other Address:* *Discipline of Chemical Engineering, School of Engineering, University of KwaZulu-Natal, Howard Colle.ge. Campus, King Ge.orge. V Ave.nue., Durban 4041, SOUTH AFRICA*
1021-9986/2022/2/569-581 16/$/6.06

has become a crucial topic because of its importance in the energy and environmental fields. The separation of CH_4 and CO_2 mixtures is particularly relevant in the purification of conventional natural gas and coal steam methane [1], unconventional shale gas, and the treatment of anaerobic gas from biomass, all of which contain fairly high amounts of CO_2 [2].

Conventionally, natural gas is purified using gas absorption processes which may involve physical absorption using solvents (polycarbonate., tributylphosphate., e.tc.). However, the by-products from side reactions of solvent with some natural gas components are difficult to be disposed especially at offshore purification plants[3]. Meanwhile, conventional chemical absorption endures several drawbacks such as flooding, foaming, channeling, and high capital costs. Besides the absorption technology, various potential technologies such as adsorption and membrane separation have been studied to separate. CO_2 from natural gas[3]. In the adsorption technology, silica-alumina adsorbent combined with Pressure Swing Adsorption (PSA) has been adopted [4]. Among these methods, membrane technology is the most attractive one from novelty, energy consumption, minimum required space, and minimum environmental pollution points of view. In the last decades, extensive studies have been conducted in the area of membrane separation. Among various types of membranes, polymeric ones have some advantages such as ease of processing and suitable strength for natural gas sweetening. The most commonly used commercial polymers for gas separation are the phenyl groups based polysulfone (PSf), polyethersulfone (PES), and aromatic polyimide (PI)[4]. PSf and PES are high-performance synthetic glassy polymers that have good stability, permeability, selectivity, high critical pressure of plasticization, and low cost [6]. They can be considered the standard materials used for MMMs fabrication due to their superior physical and chemical properties coupled with good separation performance. PES with desirable characteristics, CO_2/CH_4 intrinsic selectivity of 30, and appropriate. *T*g of 215 °C is a good candidate for membrane preparation. The main properties of membranes such as hydrophilicity, mechanical properties, pore size, and membrane morphology could be changed by applying a polymer mixture. However, these polymeric membranes showed less desirable separation performance due to the tradeoff between permeability and selectivity as propounded by Robeson [5]. Besides polymeric membranes, inorganic membranes, especially zeolite membranes (DDR, Silicalite-1, and SAPO-34) have been also explored in the high-pressure gas separation process. The zeolite membranes showed high selectivity towards CO_2 due to differences in diffusivity and competitive adsorption [6]. Although inorganic membranes displayed excellent separation selectivity, large-scale fabrication of these membranes is difficult as it involves expensive raw materials, complex fabrication methods, and a long preparation time. In order to overcome the limitations imposed by both polymeric membranes and inorganic membranes, the idea to formulate composite membranes has emerged in the past few decades. Mixed Matrix Membranes (MMMs) are composite polymeric membranes incorporated with an inorganic adsorbent or molecular sieve material as fillers [7].

Small pore zeolites especially SAPO-34 appeal as interesting fillers due to their high adsorption affinity to CO_2 SAPO-34 zeolite is chabazite (CHA) structure zeolite that has a 0.38 nm framework pore size; which is nearly similar to molecule sizes of the various gasses in a natural gas mixture [3]. A recent work by *Hudiono et al.* [3] described the uses of the SAPO-34 zeolite to enhance the separation performance of a neat solid polymerized room-temperature ionic liquid (poly (RTIL)) membrane. The poly (RTIL) material was used in their study because of its "wetting agent" properties, which could improve adhesion between the polymer and the zeolite particles. By adding 20 wt.% of SAPO-34 zeolite into the poly (RTIL) polymer, the CO_2/CH_4 ideal selectivity factor increased to 39, nearly 21.8% of enhancement compared to the neat membrane. A slight increment in CO_2 permeation was observed after blending SAPO-34 zeolite in poly (RTIL) membranes. On the other hand, *Jha et al.* [8] used SAPO-34 zeolite particles as the fillers to improve the separation performance of polymer polyphophazene (PPZ) membrane for CO_2 removal. For the neat PPZ membrane, the CO_2/CH_4 ideal selectivity of 15 was achieved at 22 °C, whereas, the PPZ/SAPO-34 membrane showed a slightly increased selectivity of 17.5. A more significant increment in the CO_2/CH_4 selectivity could be observed at a lower temperature due to the increased relative adsorption of CO_2 in the SAPO-34 pores and the decrease in relative diffusivity of CH_4 [8]. The CO_2 permeability for the PPZ/SAPO-34 membrane

was lower than the neat PPZ membrane due to PPZ polymer rigidification. *Zhang et al.* [31] reported the use of Matrimid® and mesoporous ZSM-5 nanoparticles (20 wt%) for MMMs. The separation selectivity of H_2/CH_4 improved from 83 to 170 *Hosseini et al.*[9] developed a MMM by mixing Matrimid® with MgO nanoparticles. The membrane was post-treated by immersion in silver solution, and the best performance was obtained at 20 wt% MgO loading after 10 days of silver treatment. The CO_2/CH_4 selectivity slightly increased from 30 to 43 *Li et al.* [10] treated A zeolite with silver by ion exchange and mixed the modified zeolite (50 wt%) with polyethersulfone. The CO_2/CH_4 selectivity increased slightly from 35 to 44 *Sadeghi et al.* [11] incorporated silica nanoparticles into a polybenzimidazole matrix. The silica nanoparticles increased the solubility but decreased the diffusivity of gases. The permeabilities of condensable gases such as CO_2 and CH_4 were higher than that of non-condensable ones such as N_2 gas *Rojey et al.* [12] synthesized MMMs using 4A zeolite (19 wt%) and Ultem ® polyetherimide. The CO_2/CH_4 selectivity improved from 14 to 35 *Vu et al.* [13] dispersed carbon molecular sieves (36 vol%) in Matrimid ® polyimide and increased the CO_2/CH_4 selectivity from 35 to 52 *Anson et al.* [14] used a mixture of acrylonitrile-butadiene-styrene copolymer and mesoporous activated carbons particles (62.4 vol%) and increased the CO_2/CH_4 selectivity from 24 to 50.

In general, MMMs composed of the polymer as the continuous phase and inorganic filler as the dispersed phase. MMMs exhibit the combined superior properties of both inorganic fillers and polymers to achieve excellent gas separation performance [15]. However, non-selective interfacial voids form in the MMMs due to the poor compatibility between the polymer and inorganic fillers, resulting in a profound impact on the separation performance [16]. Silane coupling agents were commonly proposed to improve the compatibility of zeolite in a polymeric matrix. Silane coupling agents are silicon-based chemicals that contain two types of reactive groups, namely inorganic and organic groups in the same molecule. The general formula of a silane coupling agent is R- $(CH_2)n$-Si-X_3 in which X is a hydrolyzable group, such as methoxy, ethoxy, or acetoxy, while R is an organofunctional group, such as amino, methacryloxy and epoxy. After grafting on the zeolite, the silane coupling agent acts as an effective interface, which is a complex interaction of chemical and physical factors, such as concentration gradient, expansion coefficient, and adhesion. The unique physical and chemical properties of the silane coupling agent can even prevent debonding during composite aging [17]. *Pechar et al.* [18] reported the use of 3-aminopropyltrimethoxysilane (APTMS) to modify ZSM-2 zeolite before blending into polyimide membranes. *Pechar et al* further used silanated zeolite L filler modified with 3-aminopropyltriethoxysilane (APTES) to prepare polyimide MMMs. Both CO_2 selectivity and permeability of the modified MMM dropped relative to the neat membrane. The reduction of CO_2 adsorption indicated the zeolite pores were also partially blocked by APTES. Instead of using toluene as the solvent in the silane modification, *Mansourizadeh et al.* [19] modified zeolite 4A using APTES in EtOH. Besides the good compatibility between the modified zeolite and PU membrane was observed, a great improvement in the CO_2 selectivity was achieved. However, the CO_2 permeability was reduced by nearly 80% compared to the neat PES membrane. The reduction of permeability can only be explained by polymer rigidification [20].

To our best knowledge, not much research work focuses on the silane modification of SAPO zeolites to prepare MMMs for CO_2 separation. Based on the detailed literature review, modification of SAPO zeolite using silane has a great potential to further enhance the CO_2 separation of MMMs. The pore diameter of SAPO 34 is 0.38 nm, which is larger than the kinetic diameters of CO_2 (0.33 nm) and equal to the kinetic diameters of CH_4 (0.38 nm). Therefore, SAPO 34 is considered to be a useful filler for CO_2/CH_4 separation. Meanwhile, several MMMs with SAPO 34 have shown improved CO2 separation performance from CH4. Different functional groups were introduced onto the surface of SAPO 34 particles through the chemical reaction between 3 3-aminopropylmethyldiethoxysilane (APMDES) and SAPO 34. APMDES is a rubbery polymer having high gas permeability, good adhesion with fillers, and low selectivity. PDMS has also got low surface tension, excellent adhesion property, and the ability to fill non-selective voids. PDMS coating helps to improve the gas selectivity by filling the defects and pinholes. Therefore it is extensively used as a coating material in many gas separation membranes and in industrial coatings.

EXPERIMENTAL SECTION

Poly(ethersulfone) (PES) in powder form of Mw = 30,000 Da and density of 1.37 g/cm^3 (Sigma Aldrich Company, Germany) was selected as a membrane material because of its commercial availability, processing ease, favorable selectivity permeability characteristics, and good mechanical and thermal properties. The N-methyl-pyrolidone (NMP, obtained from Merck) was used as solvent since it is known as a green solvent and it has a low evaporation rate and low toxicity 3 3- aminopropylmethyldiethoxysilane (APMDES), aluminum isopropoxide ($Al(OPr)_3$), H_3PO_4, TEOS (99.9% purity) and isopropanol (IPA) were purchased from Merck Company (Germany). All chemicals were used as received.

Synthesis of SAPO-34 zeolite

SAPO-34 molecular sieves were synthesized by hydrothermal according to previous work[21]. The molar ratio of the starting gel was 1.0 Al_2O_3: 1.0 P_2O_5: 0.6 SiO_2: 2 SDA(s): 70 H_2O. SDA shows the composition of structure-directing agents TEAOH: Morpholine: DEA: TEA (1.0: 0.4: 0.4: 0.2). At first, the mixture of aluminum isopropoxide, deionized H_2O, and SDA were stirred until a homogeneous solution was obtained. Then the source of silica (TEOS) was added and stirred. Finally, H_3PO_4 was added dropwise to the above stirring solution. The resulting gel was further stirred for an hour. For crystallization, the initial gel was sealed in a stainless steel autoclave and then heated in an oven at 200 °C for 14 h. After this step, the solid product was cooled at room temperature. It was also centrifuged and washed several times with distilled H_2O to collect the product and then dried at 115 °C. In the end, calcination was carried out in the air at 560 °C for 5 h to remove organic template(s) molecules.

Grafting of organosilanes on SAPO-34

In the silane modification preparation, the reaction solution was planned according to the literature [22]. 1 g dried SAPO-34 powder was added to 100 mL mixture of IPA, DI H_2O, and HCl with a volume ratio of 19 IPA:H_2O:0.02 HCl and sonicated. The mixture was then placed in a round bottom flask. After 2 h stirring, the required amount of APMDES (0.1mL) was added dropwise via a syringe to the mixture under stirring. The mixture was then refluxed under an argon purge at ambient temperature for 24 h. After reaction completion, the mixture was washed several times with 500 mL anhydrous EtOH, centrifuged for 15 min at 7000 rpm and oven-dried at 80 °C overnight

Membrane preparation

The PES flakes were dried in an oven at 120 °C for 24 h in order to remove the absorbed moisture prior to the dope solution preparation. The neat PES polymeric membrane was synthesized by using 20 wt % polymers and this is based on the solvent weight. First of all, 63 mL of NMP and 15 mL of EtOH (as a non-solvent additive) were added to a 250 mL bottle with an air-tight cap 22 g of PES was added to this solvent gradually in small quantities under stirring until the clear solution was obtained. Afterward, the required amount of modified filler SAPO-34 was added to this solution in portions, and stirring was continued for almost 24 h to ensure the uniform distribution of the filler particles in the polymeric solution. Thereafter, the solution was put under sonication at ambient temperature for 30 min to remove any entrapped air. After the sonication, the membranes were cast immediately on glass plates with the help of a Zehntner film applicator set for the required thickness. Afterward, the glass plates having casted membranes were left for 1 min under ambient conditions and then were put in the coagulation bath having distilled H2O and then in mEtOH for 24 h each cycle to complete the phase inversion process. After coagulation, the glass plates were left under ambient conditions for 4 h and then placed carefully in the vacuum oven for 24 h at 65 °C to ensure the complete removal of solvent from the membranes. Afterward, the glass plates were carefully transferred to a desiccator for cooling and drying.

Membrane characterization

The chemical structure of the membranes was analyzed by Fourier transform infrared spectroscopy (NICOLET Magna IR 550) within the scanning frequency range of 400–4000 cm^{-1}. The thermal stability of polyurethane MMMs was investigated using ThermoGravimetric Analysis (TGA) within the temperature range of 30–800 °C at 10 °C/min, under an atmosphere of nitrogen (Mettler TOLEDO model SDTA 851). The membranes' morphologies and SAPO-34 nanocrystals' distribution were investigated by scanning electron microscopy (SEM) on a Hitachi S-4160 (Japan).

Permeation measurements

The variable-pressure/constant-volume apparatus (Model NM1390, Iran) was used to determine the permeabilities of membranes. The membrane sample with an effective area of 9.62 cm^2 was placed in a stainless steel permeation cell. The gas permeation measurement on the hollow fiber membranes was conducted using pure CH_4 and CO_2 gases with a purity of 99.99%. The gas permeation test rig contains four sections including; feeding of the gases, heating (oven), separation of the gases (permeation cell), and product collection. The membrane module was sealed with a gasket in a stainless steel cell which was fixed inside an oven. The feed gas was saturated by a humidifier before entering to membrane cell. Before the start of experiments, permeating test rig was vacuumed in order to remove moisture and contaminants. The feed pressure of gases in the feed, the stream was controlled by pressure sensors (2.600 G BD pressure sensors, accuracy of 0.25 FSO and DMP 343 BD pressure sensor, accuracy of 0.175% FSO, 1 mbar) and flow rates of gases were controlled using mass flow controllers (MKS Instruments). Temperature sensor (PT-100 sensors, accuracy of 0.1 K) was used CO_2 and CH_4 permeation of the membranes was measured at feed flow rates of the gases 200 mL/min. The pressure-normalized flux or permeance, (P_i/l) was calculated by the equation:

$$\frac{P_i}{l} = \frac{N}{\Delta P} = \frac{Q}{A \times \Delta P}\left(\frac{273.15 \times 10^6}{T}\right) \quad (1)$$

$$\alpha_{ii} = \frac{\frac{P_i}{l_i}}{\frac{P_i}{l_i}} \quad (2)$$

where (P_i/l) is the gas permeance of a membrane in GPU (1 GPU = 1 × 10^{-6} cm^3(STP)/cm^2 s cmHg), i represents the penetrating gas i, Q_i is the volumetric flow rate of gas permeated through the membrane (cm^3/s, STP), A the effective membrane area (cm^2), ΔP is the trans-membrane pressure (cm Hg), and T is the temperature at which the permeation experiment being performed. A chromatography (Perkin Elmer) was used to investigate the composition of gases side. αij represents the ideal selectivity of gas i to j.

Experimental design

Design of Experiments (DoE) software (version 11.0) was used to generate the experiment runs for CO_2 separation from the binary gas mixture. 2^3 factorial and CCD-RSM method was used to produce the experiment runs. Subsequently, the value of the distance from the axial point (α) was selected at 1 (face-centered). Table 1 displays the experimental runs produced by the software. Referring to Table 1, the first 8 runs were located at factorial points while the next 6 runs were placed at axial points Meanwhile, the last 6 runs were located at central points which were used to estimate the data reproducibility. Then, the sequence of runs was randomized to minimize the effect of the uncontrolled factors. After that, experiments were conducted based on the combination of process parameters, and then, CH_4 permeance, CO_2 permeance, and CO_2/CH_4 separation factor were obtained and included in Table 1. The data were analyzed statistically in order to develop empirical models. The empirical model of each response was defined based on equation (3) as follows.

$$y = \beta_0 + \sum_{i=1}^{k} \beta_i x_i + + \sum_{i=1}^{k} \beta_{ii} x_{ii}^2 + \sum_{i=1}^{k} \beta_{ij} x_i x_j + \varepsilon \quad (3)$$

Where y is the response (CO_2 permeation), βs are regression coefficients, x_i is a coded independent variable, ε is the error and k is the number of factors. As the last step, Analysis of Variance (ANOVA) was used through statistical analysis software for graphical analyses of the data to obtain the interaction between the process variables and the responses. The statistical significance was checked by the Fisher F-test, and model terms were evaluated by the p-value (probability) with 95% confidence level. The quality of the fit polynomial model was expressed by the coefficient of determination R^2 and adjusted R^2 in the same program[23, 24]. The optimal condition is in Table 1 entry 5.

RESULTS AND DISCUSSION

Membrane characterization

The FT-IR spectra of pure PES membrane, APMDES /SAPO-34, PES/SAPO-34/ APMDES are shown in Fig. 1. The FT-IR spectrum of pure PES membrane displayed bands at 1290 cm^{-1} and 1325 cm^{-1}, representing the presence of O=S=O stretching vibration. The adsorption peaks at 2960 cm^{-1} and 1380 cm^{-1} corresponded to C–H stretching and bending vibrations respectively.

Table 1: Experimental runs generated by CCD coupled with RSM and the results obtained.

Run	Factors (Levels)			Responses (Y)		
	Temperature (°C)	Feed pressure (bar)	CO_2 feed composition (vol%)	CO_2 permeance (GPU)	CH_4 permeance (GPU)	CO_2/CH_4 separation factor
	(A)	(B)	(C)	(Y1)	(Y2)	(Y3)
1	50	15	15	1.45	0.03	7.8
2	40	9	42.5	2.54	0.04	10.4
3	30	15	70	2.05	0.01	14.1
4	40	3	42.5	3.1	0.06	9.6
5	30	15	15	1.22	0.03	14.4
6	40	9	70	2.86	0.06	9.9
7	40	9	42.5	2.54	0.04	10.8
8	50	3	70	3.82	0.12	8.2
9	40	9	42.5	2.53	0.03	10.9
10	40	9	42.5	2.53	0.03	10.9
11	50	15	70	2.44	0.07	10.6
12	30	3	70	3.41	0.12	10.6
13	50	9	42.5	2.52	0.04	9.5
14	30	9	42.5	2.33	0.02	13.1
15	50	3	15	2.74	0.11	4.2
16	40	9	15	2.01	0.06	10.1
17	30	3	15	2.41	0.07	10.3
18	40	15	42.5	1.72	0.03	14.1
19	40	9	42.5	2.54	0.04	10.8
20	40	9	42.5	2.54	0.04	10.9

Meanwhile, the C=C stretching conjugation of benzene rings was detected at 1565 cm^{-1} [25]. The modified MMM sample exhibited analogous and comparable FT-IR spectrums to the pure PES membrane. However, intense peaks were observed in the range of 900–1200 cm^{-1} and these peaks correspond to the asymmetric vibration of Si–O or Al–O tetrahedral in the SAPO-34 filler [26]. In the range of 760–680 cm, the peaks were observed due to the various rotations and vibrations within $–(CH_2)_3–$ a group of silane. Meanwhile, the Si–O–C linkage formation contributed to the peak at 1015 cm^{-1}. However, the low concentration of silane (1 wt.%) led to undetectable peaks of C–N stretching and N–H bending vibrations in the FT-IR spectrum.

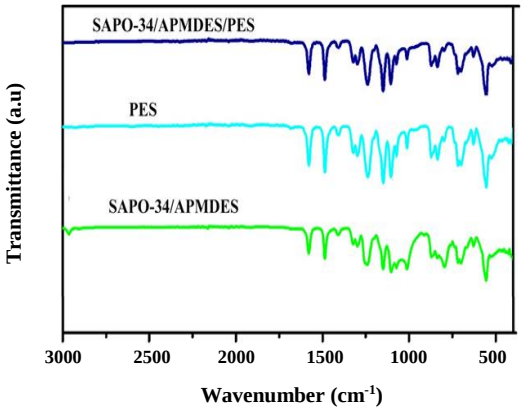

Fig. 1: FT-IR spectra of membranes.

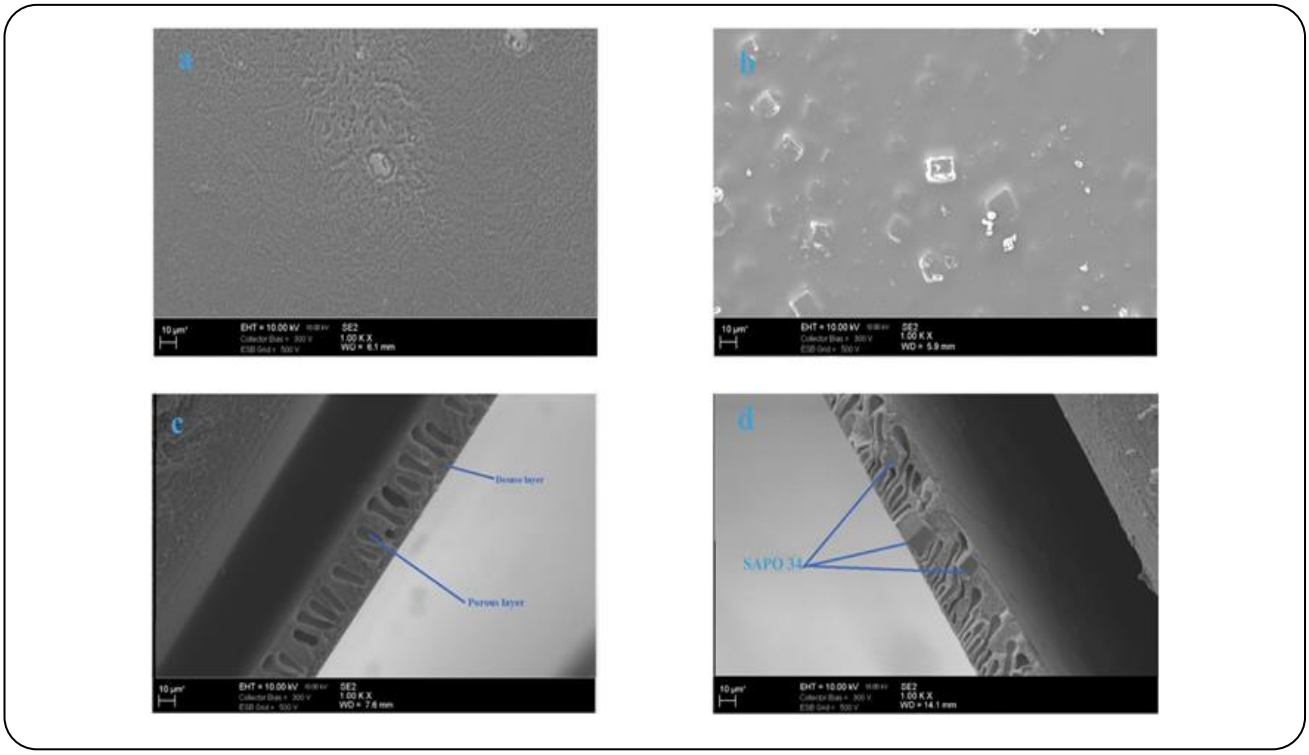

Fig. 2: Surface SEM images (a) PES membrane (b) PES/SAPO-34/ APMDES, cross-sectional SEM images (c) PES membrane (d) PES/SAPO-34/ APMDES.

Fig. 2a shows the surface of asymmetric PES membrane having surface defects or voids Fig. 2b shows the surface images of APMDES coated 30 wt.% SAPO-34 loaded PES membrane which confirms uniform distribution of SAPO-34 particles in the dense layer of the membrane. Fig. 2c shows the cross-sectional view of PES asymmetric membrane. The top dense skin layer having a thickness of 4–7 µm can be easily identified without any defects. The porous bottom layer can also be identified as having finger-like and closed cellular pores which confirms the formation of the asymmetric layer [27] Fig. 2d shows the cross-sectional view of the asymmetric PES membrane loaded with 30 wt.% SAPO-34 which proves that the crystals of SAPO- 34 have good interaction with the polymer matrix and are uniformly distributed in the top dense and bottom porous layer[28]. It has also been found that the size of finger-like pores decreases with the addition of filler particles due to the increase in the viscosity of the dope solution.

Fig. 2 shows the surface (right) and cross-sectional (left) EDX images of APMDES coated SAPO-34 loaded PES membrane indicating the light-blued color profile of silicon which confirms the presence of APMDES coating on the surface of the membrane. EDX images also indicate the red color of carbon and purple colored profile of sulfur which proves the presence of sulfone group in the form of PES [20]. The presence of SAPO-34 is confirmed by the profiles of Al (yellow) and P (green).

The texture characteristics of the filler and MMMs were investigated by using the N_2 adsorption-desorption isotherms analysis acquired at 77.3 K, as shown in (Fig. 3). The samples of SAPO-34 filler and MMMs are exposed to the process of activation prior to the N_2 adsorption-desorption analysis at 423.15 K for 5 h to remove moisture content. The results revealed that filler and MMMs samples demonstrated the type III isotherms according to the IUPAC classification indicating the wider micropores and the narrow mesopores. The steep N_2 adsorption at low relative pressure ($P/P° < 0.001$) indicates the microporous nature. of MMMs networks leading to the sharp N_2 adsorption in re.lative.ly high-pressure region ($P/P° > 0.9$) which can be attributed to the. the fact of the mild capillary condensation phenomenon of N_2 in the formation of the inter-particulate voids during the synthesis of MMMs. This is an indication of expansion. pores and flexible structure as systematically observed in soft polymeric materials.

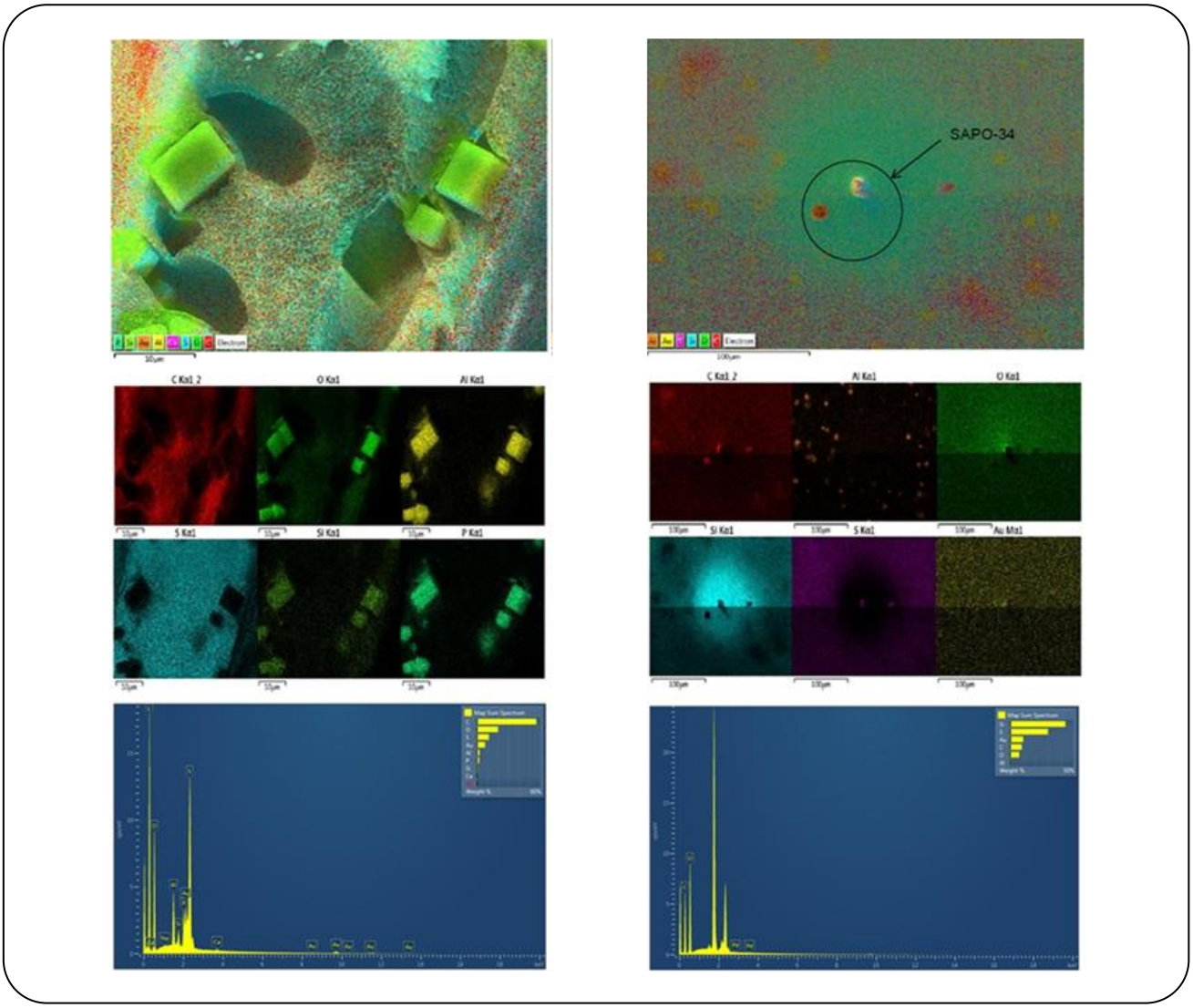

Fig. 3: EDX images of APMDES coated PES membrane filled with SAPO-34.

A small hysteresis section indicates the predominant adsorption of a gas on external surfaces. At initialization (P/P_o = 0.05– 0.35) the. monolayer gas adsorption film formed followed by the BET theory and after that in the. medium relative. pressure (P/P_o = 0.35–0.99) because. of the further adsorption which proceeds to the development of multilayers in mesopores, acting like a fluid which again demonstrates the capillary condensation phenomenon. The existence of a hysteresis loop during the desorption process in both polymer networks can also be attributed to the swelling of the polymer or elastic deformation because of gas adsorption. The specific surface area, pore. diameter and pore volume of SAPO-34 fillers are found to be 1059 m^2/g, 2.98 nm, and 0.48 cm^3/g, respectively. The specific surface area of MMMs is tabulated (Table 2). The. surface area increases with SAPO-34 addition can be. directed to the. the fact that filler particles will attach to the. PES and lead to the formation of longer networks that ultimately possess a higher specific surface area.

TGA curves of various membranes are shown in Fig. 5. TGA curve. of pure. PES membrane. shows that degradation of PES begins at 450 °C and ends at 600 °C. The TGA curve. of pure. SAPO-34 depicts that the initial weight loss of around 22% up to 105 °C is due. to the loss of hygroscopic H2O. After this, SAPO-34 is stable up to 700 °C and not appreciable. weight loss

Table 2: BET properties of MMMs.

Samples	SBET-N2 (m /g)
PES	9.85
PES/SAPO-34/ APMDE.S	17.15

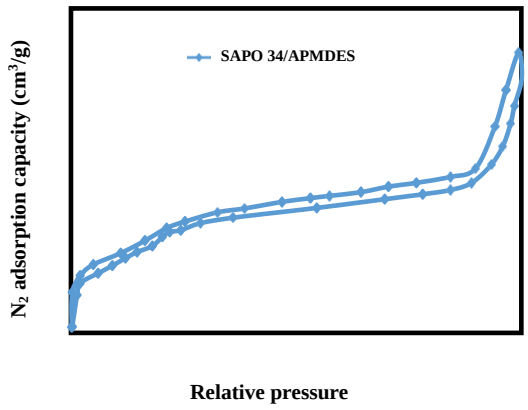

Fig. 4: N_2 adsorption-desorption analysis of SAPO-34 fille.r and MMMs.

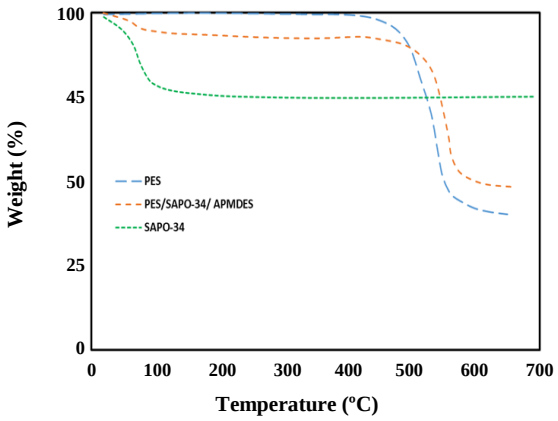

Fig. 5: TGA curves of membranes.

Is observed. TGA curves of SAPO-34 filled PES membranes show degradation temperature. keeps on shifting forward with the loading of SAPO-34. SAPO-34 loaded membranes also demonstrate initial weight loss due. to the. presence of hygroscopic moisture in SAPO-34 and this weight loss keeps on increasing with the. loading of SAPO-34[26].

CO_2/CH_4 separation results

Response surface modeling

Table 1 displays the experimental runs produced by CCD coupled with RSM and the results obtained Referring to Table 2, CO_2 and CH_4 permeances ranging from 1.22 to 3.82 GPU and 0.01 to 0.12 GPU were obtained, respectively. Meanwhile, CO_2/CH_4 separation factors ranging from 4.2 to 14.4 were achieved. All responses were reproducible with an error of ±5%.

CO_2 permeance (Y1)

The quadratic model suggested by the. DoE. software. for CO_2 permeance is shown in Equations (4(a)) and (4 (b)). Equation (4 (a)) represents the. quadratic model in the. format of coded factors. Meanwhile, actual factors of the. quadratic models are displayed in Eq. (4 (b)).

$$CO_2\,Permeance = 2.5 + 0.155A - 0.66B + 0.475C - 0.015AB + 0.03AC - 0.0325BC - 0.0223A^2 - 0.0373B^2 - 0.0123 \quad (4a)$$

$$CO_2\,Permeance = 1.6874 + 0.309T - 0.0729P + 0.016C_{FC} - 0.0003TP + 0.0001TC_{FC} - 0.00002PC_{FC} - 0.0002T^2 - 0.0011P^2 - 0.000C_{FC}^2 \quad (4b)$$

Whe.re., C_{FC}, P and T represent the CO_2 feed composition, feed pressure and temperature, respectively. Equation (4(b)) is subjected to 15 vol % < C_{FC} < 70 vol %, 3 bar < P < 15 bar and 30 °C < T < 50 °C. Subsequently, positive. and negative signs in equation 4 (a) and 4 (b) showed the synergistic and antagonistic effects of process parame.te.rs on CO_2 permeance.

Table 3 shows the ANOVA results and empirical model in terms of CO_2 permeance. Referring to Table 4, the model F-value is 170.85, while the corresponding P-value of <0.0001 was obtained for CO_2 permeance which revealed that the model is significant. Subsequently,

Table 3: ANOVA re.sults and e.mpirical mode.l te.rms of CO_2 pe.rme.ance.

Source.	Sum of squares	Degree of freedom	Me.an square.	F-value.	P-value.
Model (e.quations 4.1a and 4.1b)	6.8895	9	0.7655	170.85	<0.0001[a]
A	0.2403	1	0.2403	53.622	<0.0001
B	4.3560	1	4.3560	972.22	<0.0001
C	2.2563	1	2.2563	503.58	<0.0001
AB	0.0018	1	0.0018	0.4017	0.5404
AC	0.0072	1	0.0072	1.6070	0.2336
BC	0.0084	1	0.0084	1.8860	0.1997
A^2	0.0014	1	0.0014	0.3045	0.5932
B^2	0.0038	1	0.0038	0.8527	0.3775
C^2	0.0004	1	0.0004	0.0924	0.7673
Residual	0.0448	10	0.0045		
Lack of Fit	0.0447	5	0.0089	335.03	0.0510[b]
R^2	0.9935				
2 Adjusted R	0.9877				

a) Significant. *B) Not significant.*

F-value. of "lack of fit" of 4.44 indicated that the lack of fit is not significant. Besides, terms including, A^2, B^2, C^2, AB, AC, and BC are. the. insignificant terms. Conve.rse.ly, insignificant terms have been included in Equations (4a), (4b) (a) and 4 (b) to retain the hierarchy of the. model Besides, R^2 value. of 0.99 was obtained which confirmed the precision of the model for CO_2 permeance. Furthermore., feed pressure (te.rm B) exhibited the highest F-value. of 972.22. This result showed that feed pressure has the. most significant effect on CO_2 permeance. Meanwhile, second-order (AC and BC) and two-level (A^2, $B^{2,}$ and C^2) terms of the empirical model remained ineffective over the CO_2 permeance of PES/SAPO-34/ APMDES membrane.

Fig. 6, Fig. 7, and Fig. 8 show the influence. of feed pressure., temperature, and CO_2 feed composition on CO_2 permeance over PES/SAPO-34/ APMDES. Based on Fig. 4, when feed pressure. increases, CO_2 permeance decreases. This result could be due to the dual-sorption properties of polymer which reduced the CO_2 solubility coefficient on the. increment of feed pressure [29]. However, CO_2 permeance was enhanced on the increment of temperature. The. increasing trend of CO_2 permeance

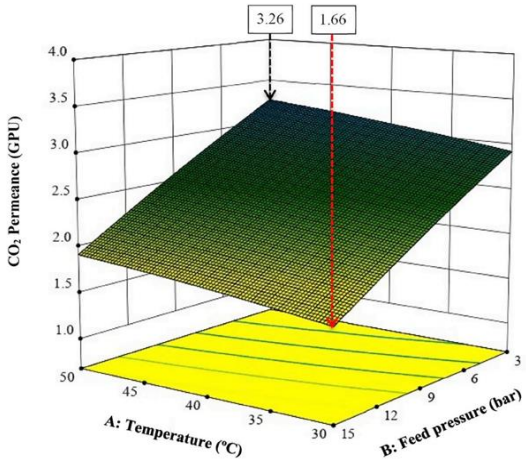

Fig. 6: Effect of temperature and feed pressure on CO_2 permeance at CO_2 feed composition of 42.5 vol%.

could be because of the. increment of CO_2 diffusivity along with the elevation of temperature [30]. In addition, the flexibility of the polymer matrix was increased which expands the. accessible Cavities [31].

Fig. 7 illustrates the. influence of CO_2 feed composition and temperature on CO_2 permeance over the

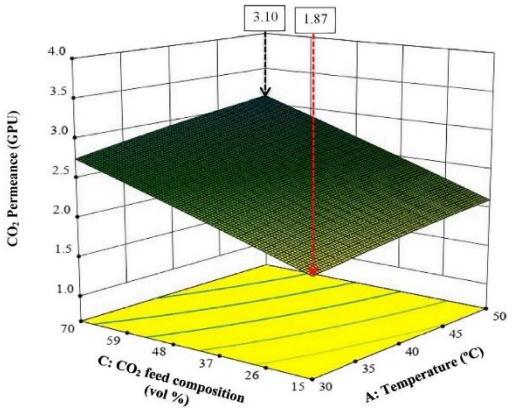

Fig. 7: Effect of temperature and CO2 feed composition on CO2 permeance at feed pressure. of 9 bar.

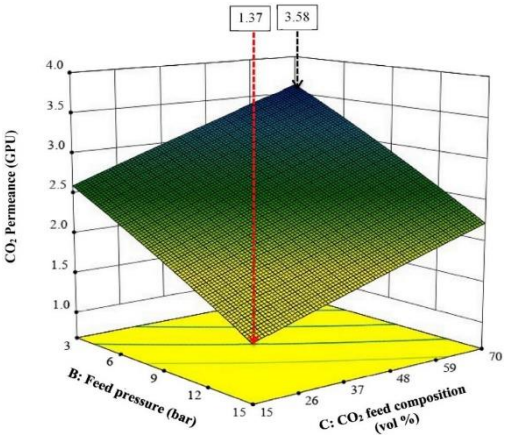

Fig. 8: E.ffe.ct of fe.e.d pre.ssure. and CO2 fe.e.d composition on CO2 pe.rme.ance. at te.mpe.rature. of 40 °C.

PES/SAPO-34/ APMDE.S at 9 bar. Based on Fig. 5, CO_2 permeance increases with the increment of CO_2 feed composition. Maximum CO_2 permeance. of 3.10 GPU is obtained at CO_2 feed composition of 70 vol% and temperature of 50 °C. This occurrence could be because of the increment of driving force when CO_2 molecules penetrated through the. PES/SAPO-34/ APMDE.S Besides, from Fig. 5, it can be observed that increasing trend of CO_2 permeance. with temperature. is similar to the results shown in Fig. 4. However, minimum CO_2 permeance. of 1.87 GPU was achieved at CO_2 feed composition of 15 vol% and a temperature of 30 °C.

Fig. 8 displays the. influence of CO_2 feed composition and feed pressure. over CO_2 permeance at 40 °C. From Fig. 6, it can be observed that the. CO_2 permeance is decreased on the increment of feed pressure at 40 °C. The decreasing trends of CO_2 permeance were mainly because of the combined effect of dual-sorption properties and thermodynamic instability of particles which reduced the CO_2 permeation polymer matrix [31]. Next, the. increase. of CO_2 permeance. with CO_2 feed composition at 40 °C is similar to the results shown in Fig. 5.

CO_2/CH_4 separation factor (Y3)

The. quadratic model suggested by the DoE. software for the response of CO_2/CH_4 separation factor is shown in Equations (5 (a)) and (5 (b)). Equation (5 (a)) represents the quadratic model in the. format of coded factors while., Equation (5 (b)) displays the. actual factors of the quadratic model.

$$CO_2/CH_4\ \text{separation factor} = 11.03 - 2.23A + 1.77B + 0.692C - 0.2575AB + 0.88AC - 0.1850BC - 0.0051A^2 + 0.4532B^2 - 1.38C^2 \quad (5a)$$

$$CO_2/CH_4\ \text{separation factor} = 16.58 - 0.2789T + 0.2875P - 0.0625C_{FC} - 0.0043TP + 0.0032TC_{FC} - 0.0011PC_{FC} - 0.0005T^2 + 0.0125P^2 - 0.0018C_{FC}^2 \quad (5b)$$

Where Eq.(5b) is subjected to 15 vol % < C_{FC} < 70 vol %, 3 bar < P < 15 bar and 30 °C < T < 50 °C. Table. 4 shows the. ANOVA result and empirical model terms of CO_2/CH_4 separation factor. The f-value. of 28.33 is shown in Table. 3 revealed that the. quadratic model is significant. Subsequently, R^2 value of 0.96 denotes that the empirical model is acceptable at the. the confidence level of 96% for the prediction of CO_2/CH_4 separation factor of PES/SAPO-34/ APMDES. Besides, A, B, C, AC, and C^2 are significant model terms. In addition, the highest The F-value of B term of 126.91 indicated that the feed pressure has the most substantial influence on the separation factor. Furthermore, the "lack of fit F-value." confirmed that the chances for lack of fit are. minimum.

Generally, the. separation of CO_2 from CH_4 over PES/SAPO-34/ APMDE.S is mainly attributed to the a dense selective layer of the. resultant membrane and it is significantly affected by the separation process parameters [32]. Fig.s 9, 10, and 11 show the influence

Table. 4. ANOVA results and empirical model terms of CO2/CH4 s.paration factor.

Source.	Sum of squares	Degree. of freedom	Me.an square.	F-value.	P-value.
Model	99.930	9	11.103	28.337	<0.0001[a]
A	31.294	1	31.294	79.865	<0.0001
B	49.729	1	49.729	126.914	<0.0001
C	4.789	1	4.789	12.221	<0.0001
AB	0.5305	1	0.5305	1.3538	0.2716
AC	6.1952	1	6.1952	15.811	0.0026
BC	0.2738	1	0.2738	0.6988	0.4227
A^2	0.0074	1	0.0074	0.0188	0.8935
B^2	0.5648	1	0.5648	1.4414	0.2576
C^2	5.2509	1	5.2509	13.4009	0.0044
Residual	3.9183	10	0.3918		
Lack of Fit	3.6426	5	0.7285	13.21	0.0857[b]
R^2	0.9623				
^{2} Adjusted R	0.9383				

a Significant.
b Not significant.

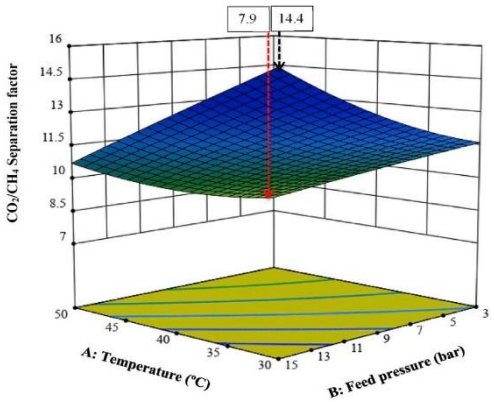

Fig. 9: Effect of temperature. and feed pressure on CO2/CH4 separation factor at CO2 feed composition of 42.5 vol%.

of feed pressure, and temperature. and CO_2 feed composition on CO_2/CH_4 separation factor. The interaction of feed pressure and temperature on the separation factor over the membrane is displayed in Fig. 9. Referring to Fig. 9, the separation factor is decreased with the elevation of temperature. This observation could be because of more. prompted diffusion of CH_4 molecules compared to the CO_2 molecules which led to the reduced separation factor with the. elevation of temperature [33].

Furthermore, Fig. 10 displays the. influence of temperature and CO_2 feed composition on CO_2/CH_4 separation factor of PES/SAPO-34/ APMDE.S at constant feed pressure. of 9 bar. Referring to Fig. 10, the separation factor is enhanced with the increment of CO_2 feed composition from 15 vol% to 42.5 vol%. Therefore., the. maximum separation factor of 11.8 is achieved at CO_2 feed composition of 42.5 vol% and temperature. of 30 °C. However, further increment of CO_2 feed composition from 42.5 vol% to 70 vol% led to the. saturation of amine–CO_2 interaction which aggregated CO_2 on the feed side. of membrane and thus, reduced the CO_2/CH_4 separation factor. In addition, higher CO_2 feed composition could swell the polymer matrix which resulted in the. increment of CH_4 penetration rate. through the PES/SAPO-34/ APMDE.S and thus, CO_2/CH_4 separation factor was dropped [34].

It can be. also observed from Fig. 10 that CO_2/CH_4 separation factor was significantly dropped on the increment of temperature at CO_2 feed composition of 15 vol% Meanwhile, at higher CO_2 feed composition of

Table 5: Comparison of CO2/CH4 mixed gas separation performance. of PES/SAPO-34/ APMDE.S fabricated in the present work with the results reported in the literature.

	Temperature (°C)	Feed pressure (bar)	CO_2 permeance (GPU)	CH_4 permeance (GPU)	CO_2/CH_4 separation factor	Ref.
PE.S/SAPO-34/ APMDE.S	30	3.0	2.85	0.242	11.8	This work
[b] Zeolite β/PES	25	3.0	0.21	0.015	13.8	[36]
[b] HSSZ-13/PES	30	3.0	2.30	–	10.1	[37]
[b] ZIF-94/PES	35	3.5	2.71	–	9.6	[38]

a CO_2 feed composition is 42.5 vol%.
b CO_2 feed composition is 50%.

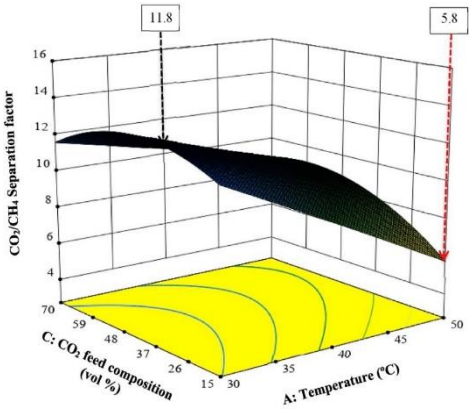

Fig. 10: Effect of temperature and CO2 feed composition on CO2/CH4 separation factor at feed pressure. of 9 bar.

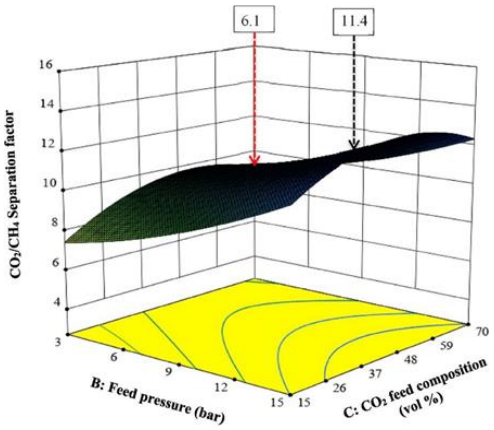

Fig. 11: Effect of feed pressure and CO2 feed composition on CO2/CH4 separation factor at the temperature of 40 °C.

70 vol%, CO_2/CH_4 separation factor was slightly reduced when the temperature increased. At low CO_2 feed composition of 15 vol%, the. presence. of a higher amount of CH_4 in the feed, reducing the CO_2 adsorption-diffusion rate. and thus, decreased the. CO_2/CH_4 separation factor [35]. From the. results obtained, that a minimum CO_2/CH_4 separation factor of 5.8 was achieved at a temperature of 50 °C and CO_2 feed composition of 15 vol%.

On the other hand, Fig. 11 displays the. influence of CO_2 feed composition and feed pressure on CO_2/CH_4 separation factor of PES/SAPO-34/ APMDE.S at a constant temperature of 40 °C. Based on Fig. 9, a maximum CO_2/CH_4 separation factor of 11.4 is obtained at a feed pressure of 15 bar and CO_2 feed composition of 42.5 vol%. Meanwhile, a minimum CO_2/CH_4 separation factor of 6.1 is found at CO_2 feed composition of 70 vol% and feed pressure of 3 bar.

Comparison of mixed gas separation performance of PES/SAPO-34/ APMDES with reported literature

Table. 5 shows the. comparison of mixed gas separation performance of PES/SAPO-34/ APMDE.S fabricated in the current work with the results reported in the literature. Referring to Table 4, PES/SAPO-34/ APMDE.S fabricated in the. present work exhibited higher CO_2 permeance compared to those values reported in the literature for zeolite β, HSSZ-13, and ZIF-94 based PE.S. Hence, this comparison study revealed that the PES/SAPO-34/ APMDES fabricated in the present work is the potential for CO_2 separation processes.

This comparison has been drawn on Robeson's upper bound limits for CO_2/CH_4 and CO_2/N_2 gas pairs as shown in Fig. 12. It has been found that for pure. gas permeation results, the. performance. of PDMS coated 30 wt.% SAPO-34 PES membrane surpasses the present upper bound limit 2008

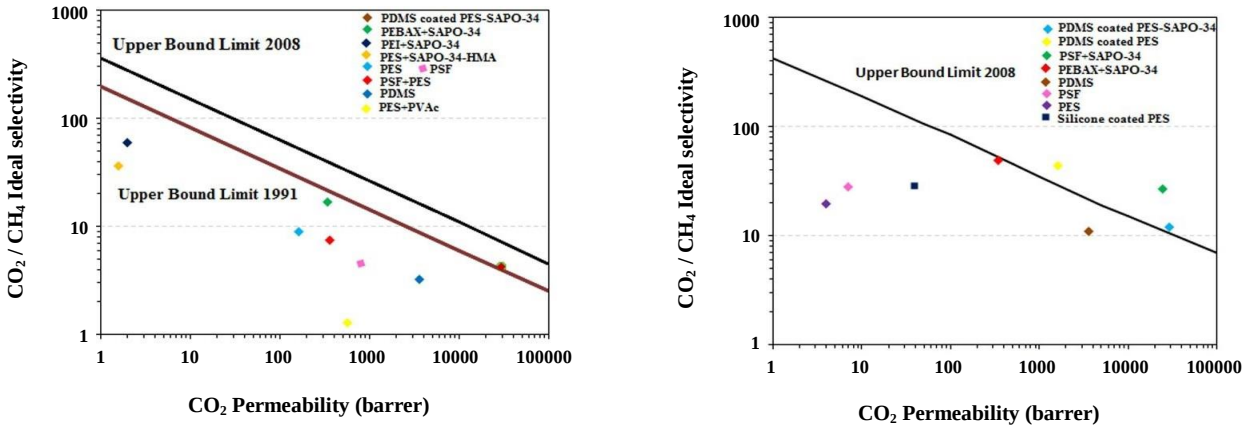

Fig. 12: Comparison of gas permeation properties with Robeson upper bound limit.

at 20 bar and 25 °C for CO_2/N_2 whereas for CO_2/CH_4, it crosses the previous upper bound limit 1991.

CONCLUSIONS

In summary, SAPO-34 seeds and membranes were functionalized with APMDE.S. APMDE.S was selected as the. silane. coupling agent instead of the. another ethoxy group-based silane. in this work because. the. methoxy group is more. vulnerable. to hydrolysis and it possesses less steric hindrance. as compared to ethoxy group. The. successful incorporation of APMDE.S in the. SAPO-34 framework was confirmed by FTIR. The. chabazite. structure. of SAPO-34 was preserved after the. functionalization step. It was found that SAPO-34 incorporated MMMs enjoyed an enhanced morphology and thermal stability as revealed by FE.SE.M and TGA testing techniques. The. interaction of process parameters including, CO_2 feed composition, feed pressure, and temperature have been studied over PES/SAPO-34/ APMDE.S for CO_2 separation from CO_2/CH_4 binary gas mixture. using the Design of Experiment (DoE). The results showed that the. increment of temperature reduced the CO_2/CH_4 separation factor while the elevation of feed pressure enhanced the separation factor of PES/SAPO-34/ APMDES. Furthermore, the elevation of CO_2 feed composition to 42.5 vol% increased the separation factor, However, a further increase in CO_2 feed composition from 42.5 vol% to 70 vol% reduced the separation factor. The. results also showed that feed pressure was the most significant process parameter that intensely affected the responses compared to the other process parame.te.rs. Overall, the. study on the interaction between the process parame.te.rs on CO_2 separation from CO_2/CH_4 binary gas mixture over PES/SAPO-34/ APMDE.S have. been achieved. The. findings subsequently demonstrated the MMM potential in gas separation and strengthened our knowledge of membrane technology.

Although the. progress and success of gas separation membranes have. been witnessed in the. past, there are. huge. demands for better membranes in order to compete with conventional processes such as cryogenic distillation and adsorption/absorption. Therefore., we outline the following key areas for future research and studies.

(1) Polymeric membranes containing nanoparticles are. promising candidates to circumvent the trade-offs between permeability vs. selectivity of polymeric materials and between aging/plasticization rates vs dense-layer thickness.

(2) Simplification and scale-up of current fabrication processes for membranes, particularly for membranes containing nanoparticles, should be. promoted in order to produce cost-effectiveness. membrane. products.

(3) Novel strategies to conduct crosslinking or annealing modifications at the specific dense-selective layer without damaging the. substrate structure. are. needed to facilitate. the. fabrication of membranes with improved anti-aging and anti-plasticization characteristics.

(4) MMs membranes comprising polymeric layers(s) and inorganic layer(s) provide another opportunity and direction for the future. research and development.

(5) Long-te.rm stability studies and data in the. range. of 3–5 years are. vital and imperative. to expand TFC

membranes for industrial applications.

(6) Exploration of new applications is encouraged to take full advantage of MMs membranes.

Received : Ju.y 16, 2020 ; Accepted : Nov. 2, 2020

REFERENCES

[1] Pera-Titus M., Porous Inorganic Membranes for CO_2 Capture: Present and Prospects, *Chemical Reviews*, **114(2)**: 1413-1492 (2014).

[2] Li B., Duan Y., Luebke D., Morreale B., Advances in CO_2 Capture Technology: A Patent Review, *Applied Energy*, **102**: 1439-1447 (2013).

[3] Hudiono Y.C., Carlisle T.K., LaFrate A.L., Gin D.L., Noble R.D., Novel Mixed Matrix Membranes Based on Polymerizable. Room-Temperature Ionic Liquids and SAPO-34 Particles to Improve CO_2 Separation, *Journal of Membrane Science*, **370(1-2)**: 141-148 (2019).

[4] Scholes C.A., Smith K.H.,Kentish S.E., Stevens G.W., CO_2 Capture from Pre-Combustion Processes - Strategies for Membrane Gas Separation, *International Journal of Greenhouse Gas Control*, **4(5)**: 739-755 (2020).

[5] Robeson L.M., The Upper Bound Revisited, *Journal of Membrane Science*, **320(1-2)**: 390- 400 (2018).

[6] Carreon M.A., Li Sh., Falconer J.L., Noble R.D., Alumina-Supported SAPO-34 Membranes for CO_2/CH_4 Separation, *Journal of the American Chemical Society*, **130(16)**: 5412-5413 (2018).

[7] Nik O.G., Chen X.Y., Kaliaguine S., Amine-Functionalized Zeolite FAU/E.MT-Polyimide Mixed Matrix Membranes for CO_2/CH_4 Separation, *Journal of Membrane Science*, **379(1-2)**: 468-478 (2019).

[8] Jha P., Way J.D., Carbon Dioxide Selective Mixed-Matrix Membranes Formulation and Characterization Using Rubbery Substituted Polyphosphazene, *Journal of Membrane Science*, **324(1-2)**: 151-161 (2018).

[9] Hosseini S.S., Li Y., Chung T.Sh., Liu Y., Enhanced Gas Separation Performance. of Nanocomposite Membranes Using MgO Nanoparticles, *Journal of Membrane Science*, **302(1-2)**: 207-217 (2017).

[10] Li Y., Chung T.S., Kulprathipanja S., Novel Ag^+-Zeolite/Polymer Mixed Matrix Membranes with a High CO_2/CH_4 Selectivity, *AIChE Journal*, **53(3)**: 610-616 (2017).

[11] Sadeghi M., Semsarzadeh M.A., Moadel H., Enhancement of the Gas Separation Properties of Polybenzimidazole (PBI) Membrane by Incorporation of Silica Nano Particles, *Journal of Membrane Science*, **331(1-2)**: 21-30 (2019).

[12] Rojey A., et al., Process for Separation of the. constituents of a Mixture in the Gas Phase Using a Composite Membrane. Process for Separation of the Constituents of a Mixture in the Gas Phase Using a Composite Membrane, (2020).

[13] Vu D.Q., Koros W.J., Miller S.J., Mixed Matrix Membranes Using Carbon Molecular Sieves: I Preparation and Experimental Results, *Journal of Membrane Science*, **211(2)**: 311-334 (2003).

[14] Anson M., Marchese J., Garis E., Ochoa N., Pagliero C., ABS Copolymer-Activated Carbon Mixed Matrix Membranes for CO_2/CH_4 Separation, *Journal of Membrane Science*, **243(1-2)**: 19-28 (2020).

[15] Şener T., Okumuş E., Gürkan T., Yilmaz L., The Effect of Different Solvents on the. Performance of Zeolite-Filled Composite. Pervaporation Membranes, *Desalination*, **261(1-2)**: 181-185 (2010).

[16] Chen X.Y., Vinh-Thang H., Rodrigue D., Kaliaguine S., Amine-Functionalized MIL-53 Metal-Organic Framework in Polyimide Mixed Matrix Membranes for CO_2/CH_4 Separation, *Industrial and Engineering Chemistry Research*, **51(19)**: 6895-6906 (2012).

[17] Ismail A.F., Kusworo T.D., Mustafa A., Enhanced Gas Permeation Performance of Polyethersulfone Mixed Matrix Hollow Fiber Membranes Using Novel Dynasylan Ameo Silane Agent, *Journal of Membrane Science*, **319(1-2)**: 306-312 (2018).

[18] Pe.char T.W., Kim S., Vaughan B., Marand E., Tsapatsis M., Jeong K., Cornelius C.J., Fabrication and Characterization of Polyimide-Zeolite L Mixed Matrix Membranes for Gas Separations, *Journal of Membrane Science*, **277(1-2)**: 195-202 (2006).

[19] Mansourizadeh A., Ismail A.F., Effect of Additives on the Structure and Performance. of Polysulfone Hollow Fiber Membranes for CO_2 Absorption, *Journal of Membrane Science.*, **348(1-2)**: 260-267 (2010).

[20] Hillock A.M.W., Miller S.J., Koros W.J., Crosslinked Mixed Matrix Membranes for the Purification of Natural Gas: Effects of Sieve Surface Modification, *Journal of Membrane Science*, **314(1-2)**: 193-199 (2018).

[21] Li S., Alvarado G., Noble R.D., Falconer J.L., Effects of Impurities on CO_2/CH_4 Separations Through SAPO-34 Membranes, *Journal of Membrane Science*, **251(1-2)**: 59-66 (2005).

[22] Damayanti N.P., Preparation of Superhydrophobic PET Fabric from Al_2O_3-SiO_2 Hybrid: Geometrical Approach to Create High Contact Angle Surface from Low Contact Angle Materials, *Journal of Sol-Gel Science and Technology*, **56(1)**: 47-52 (2020).

[23] Alizadeh M., Sadrameli S.M., Indoor Thermal Comfort Assessment Using PCM Based Storage System Integrated with Ceiling Fan Ventilation: Experimental Design and Response Surface Approach, *Energy and Buildings*, **188-189**: 297-313 (2019).

[24] Alizadeh M., Sadrameli S.M., Numerical Modeling and Optimization of Thermal Comfort in Building: Central Composite Design and CFD Simulation, *Energy and Buildings*, **164**: 187-202 (2018).

[25] Junaidi M.U.M.,Leo C.P., Kamal S.N.M., Ahmad A.L., Chew T.L., Carbon Dioxide Removal from Methane by Using Polysulfone/SAPO-44 Mixed Matrix Membranes, *Fuel Processing Technology*, **112**: 1-6 (2019).

[26] Leo C.P., Ahmad Kamil N.H., Junaidi M.U.M., Kamal S.N.M., Ahmad A.L., The Potential of SAPO-44 Zeolite Filler in Fouling Mitigation of Polysulfone Ultrafiltration Membrane, *Separation and Purification Technology*, **103**: 84-91 (2019).

[27] Aroon M.A., Ismail A.F., Matsuura T., Montazer Rahmati M.M., Performance Studies of Mixed Matrix Membranes for Gas Separation: A Review, *Separation and Purification Technology*, **75(3)**: 229-242 2010.

[28] Favvas E.P., Stefanopoulos K.L., Nolan J.W., Papageorgiu S.K., Mitropoulos A.Ch., Lairez D., Mixed Matrix Hollow Fiber Membranes with Enhanced Gas Permeation Properties, *Separation and Purification Technology*, **132**: 336-345 (2014).

[29] Zhuang G.L., Tseng H.H., Uchytil P., Wey M.Y., Enhancing the CO_2 Plasticization Resistance of PS Mixed-Matrix Membrane by Blunt Zeolitic Imidazolate Framework, *Journal of CO_2 Utilization*, **25**: 79-88 (2018).

[30] Bos A., Pünt I.G.M., Wessling M., Strathmann H., CO_2-Induced Plasticization Phenomena in Glassy Polymers, *Journal of Membrane Science*, **155(1)**: 67-78 (1999).

[31] Molki B., Mohammadi Aframehr W., Bagheri R., Salimi J., Mixed Matrix Membranes of Polyurethane with Nickel Oxide Nanoparticles for CO_2 Gas Separation, *Journal of Membrane Science*, 2018. **549**: p. 588-601.

[32] Mubashir M., Yeong Y.F., Leng Chew T., Lau K.K., Comparison of Post-Treatment Methods on the Performance of Hollow Fiber Membranes Containing Metal Organic Framework in Gases Separation, *Industrial and Engineering Chemistry Research*, **58(17)**: 7120-7130 (2019).

[33] Oyama S.T., Stagg-Williams S.M., Inorganic, Polymeric and Composite. Membranes: Structure., Function and other Correlations, Inorganic, Polymeric, and Composite. Membranes: Structure-Function and Other Correlations, (2011).

[34] Falbo F., et al., CO Separation by Means of Matrimid Hollow Fibre Membranes, *Appl. Petrochem Res.*, **6**: 439-450 (2016).

[35] Rodenas T., Dalen M., Serra-Crespo P., Kapteijn F., Gascon J., Mixed Matrix Membranes Based on NH2-functionalized MIL-type MOFs: Influence. of Structural and Operational Parameters on the CO 2/CH4 Separation Performance, *Microporous and Mesoporous Materials*, **192**: 35-42 (2014).

[36] Li Y., Chung T.Sh., Huang Z., Kulprathipanja S., Dual-Layer Polyethersulfone (PE.S)/BTDA-TDI/MDI co-polyimide. (P84) Hollow Fiber Membranes with a Submicron PES-Zeolite Beta Mixed Matrix Dense-Selective Layer for Gas separation, *Journal of Membrane Science*, **277(1-2)**: 28-37 (2006).

[37] Husain S., Koros W.J., Mixed Matrix Hollow Fiber Membranes Made with Modified HSSZ-13 Zeolite in Polyetherimide Polymer Matrix for Gas Separation, *Journal of Membrane Science*, **288(1-2)**: 195-207 (2007).

[38] Etxeberria-Benavides M., et al., High Performance Mixed Matrix Membranes (MMMs) Composed of ZIF-94 Filler and 6FDA-DAM Polymer, *Journal of Membrane Science*, **550**: 198-207 (2018).